Research paper

The last mangroves of Marajó Island — Eastern Amazon: Impact of climate and/or relative sea-level changes

Marlon C. França [a,c,*], Mariah I. Francisquini [d], Marcelo C.L. Cohen [a,b], Luiz C.R. Pessenda [d], Dilce F. Rossetti [e], José T.F. Guimarães [a], Clarisse B. Smith [a]

[a] Coastal Dynamics Laboratory, Post-Graduate Program in Geology and Geochemistry, Federal University of Pará, Av. Perimentral 2651, Terra Firme, CEP: 66077-530, Belém (PA), Brazil
[b] Faculty of Oceanography, Federal University of Pará, Rua Augusto Corrêa, n 1, Guama, CEP: 66075-110, Belém (PA), Brazil
[c] Federal Institute of Pará, Av. Almirante Barroso, 1155, Marco, CEP: 66090-020, Belém (PA), Brazil
[d] Center for Nuclear Energy in Agriculture (CENA), University of São Paulo, 13400-000, Piracicaba (SP), Brazil
[e] National Space Research Institute (INPE), Rua dos Astronautas 1758-CP 515, CEP: 12245-970, São José dos Campos (SP), Brazil

ARTICLE INFO

ABSTRACT

The dynamics, over the last 7500 years, of a mangrove at Marajó Island in northern Brazil were studied by pollen and sedimentary facies analyses using sediment cores. This island, located at the mouth of the Amazon River, is influenced by riverine inflow combined with tidal fluctuations of the equatorial Atlantic Ocean. Herbaceous vegetation intermingled with rainforest dominates the central area of the island, while várzea is the main vegetation type along the littoral. In particular, the modern northeastern coastal zone is covered by a mosaic of dense rainforest, herbaceous vegetation, mangroves, várzea, and restinga. The integration of pollen data and facies descriptions indicates a tidal mud flat colonized by mangroves in the interior of Marajó Island between ~7500 cal yr BP and ~3200 cal yr BP. During the late Holocene, mangroves retracted to a small area (100–700 m in width) along the northeastern coastal plain. Mangrove expansion during the early and mid Holocene was likely caused by the post-glacial sea-level rise which, combined with tectonic subsidence, led to a rise in tidal water salinity. Salinity must have further increased due to low river discharge resulting from increased aridity during the early and mid Holocene. The shrinking of the area covered by mangrove vegetation during the late Holocene was likely caused by the increase in river discharge during the late Holocene, which has maintained relatively low tidal water salinity in Marajó Island. Tidal water salinity is relatively higher in the northeastern part of the island than in others, due to the southeast–northwest trending current along the littoral. The mixing of marine and riverine freshwater inflows has provided a refuge for mangroves in this area. The increase in flow energy during the last century is related to landward sand migration, which explains the current retraction of mangroves. These changes may indicate an increased exposure to tidal influence driven by the relative sea-level rise, either associated with global fluctuations or tectonic subsidence, and/or by an increase in river water discharge.

© 2012 Elsevier B.V. All rights reserved.

1. Introduction

Mangroves are highly susceptible to climatic changes and sea-level oscillations (e.g., Fromard et al., 2004; Versteegh et al., 2004; Alongi, 2008; Berger et al., 2008; Cohen et al., 2012). They have been almost continuously exposed to disturbance as a result of fluctuations in sea-level over the last 11,000 years (Gornitz, 1991; Blasco et al., 1996; Sun and Li, 1999; Behling et al., 2001; Lamb et al., 2006; Alongi, 2008; Berger et al., 2008; Cohen et al., 2008; Gilman et al., 2008). During the Holocene, the post-glacial sea-level rise and changes in river water discharge have

been considered the main driving forces behind the expansion/contraction of mangroves in northern Brazil (Cohen et al., 2008; Lara and Cohen, 2009; Guimarães et al., 2010; Smith et al., 2012). However, important changes in coastal morphology have been recorded in this region as a result of tectonic reactivations, which could have modified the relative sea-level (RSL), with a potential impact on mangrove distribution (Rossetti et al., 2007; Miranda et al., 2009; Rossetti et al., 2012).

An empirical model based on an ecohydrological approach, which allows the integration of hydrographical, topographical and physico-chemical information with vegetation characteristics of mangroves and marshes, indicates that changes in pore water salinity affect vegetation boundaries (Cohen and Lara, 2003; Lara and Cohen, 2006). In addition to studies in northern Brazil, the relationship between mangrove distribution and sediment geochemistry has been widely studied in other coastal regions (Hesse, 1961; Baltzer, 1970; Walsh, 1974; Baltzer, 1975; Snedaker, 1982; Lacerda et al., 1995; McKee, 1995;

Pezeshki et al., 1997; Alongi et al., 1998, 1999, 2000; Clark et al., 1998; Matthijs et al., 1999; Youssef and Saenger, 1999).

Generally, mangroves are distributed parallel to the coast with some species dominating areas more exposed to the sea, and others occurring landward at higher elevations (Snedaker, 1982). This zonation is a response of mangrove species mainly to tidal inundation frequency, nutrient availability, and porewater salinity in the intertidal zone (Hutchings and Saenger, 1987).

Mangroves of the littoral of northern Brazil follow well-known patterns (Behling et al., 2001; Cohen et al., 2005a), where salinity results in the exclusion of freshwater species (Snedaker, 1978) and leads to characteristic patterns of species zonation and predictable types of community structure (Menezes et al., 2003). Mangroves are more tolerant to soil salinity than is *várzea* forest (Gonçalves-Alvim et al., 2001) and sediment salinity is mostly controlled by flooding frequency (Cohen and Lara, 2003) and estuarine gradients (Lara and Cohen, 2006).

Changes in mangrove distribution may also reflect changes in variables that control coastal geomorphology (e.g. Blasco et al., 1996; Fromard et al., 2004; Lara and Cohen, 2009). The development of mangroves is regulated by continent–ocean interactions and their expansion is determined by the topography relative to sea-level (Gornitz 1991; Cohen and Lara, 2003) and flow energy (Chapman 1976; Woodroffe et al., 1989), where mangroves preferentially occupy mud surfaces. Thus, a relative rise in sea-level may result in mangroves migrating inland due to changes in flow energy and tidal inundation frequency. Similarly, vegetation on elevated mudflats is subject to boundary adjustments, since mangroves can migrate to higher locations and invade these areas (Cohen and Lara, 2003).

The potential of each variable to influence mangrove establishment will depend on the environmental characteristics of the given littoral. Climate and hydrology are the main factors controlling the modern distribution of geobotanical units along the coast of the Amazon (Cohen et al., 2008, 2009). According to these authors, mangroves and saltmarshes dominate the marine-influenced littoral when tidal water salinity lies between 30 and 7‰ to the southeastern coastline, and *várzea* and herbaceous vegetation dominate freshwater-influenced coasts with tidal water salinity below 7‰ in the northwest. The littoral of Marajó Island, at the mouth of the Amazon River, is part of the fluvial sector (Fig. 1a) (Cohen et al., 2008; Smith et al., 2011, 2012).

The mangroves of Marajó Island are currently restricted to a relatively narrow section of the northeastern area of the island (Cohen et al., 2008; Smith et al., 2012). This mangrove has developed continuously since at least 2700 cal yr BP (Behling et al., 2004). According to pollen records from hinterland (Lake Arari), the area covered by mangrove vegetation was wider between ~7250 and ~2300 cal yr BP (Smith et al., 2011).

The purpose of this work was to study the environmental history of the northeastern part of Marajó Island, and discuss the processes that caused the contraction of the mangrove during the Holocene. We focus on vegetation development, the location of boundaries between mangrove and dry herbaceous vegetation, and areas where changes in sensitive vegetation related to RSL and tidal water salinities can be expected. This approach is based on the integration of pollen and facies analyses of five sediment cores, collected at distinct locations presently covered by mangrove, *várzea* and herbaceous vegetation.

2. Study area

The study site is located on the island of Marajó in northern Brazil, which covers approximately 39,000 km^2 (Cohen et al., 2008). The island is located at the mouth of the Amazon River (Fig. 1). Sediment cores were taken on the coastal plain of the town of Soure and from a lake surrounded by a herbaceous plain, and cores were denominated R-1, R-2, R-3, R-4 and R-5 (Table 1).

The study area covers the central-eastern part of the coastal plain. Its topographical range is less than 5 m and it extends inland to the maximum of the intertidal zone, which borders the coastal plateau (França and Sousa Filho, 2006).

2.1. Geological and geomorphological setting

The coastal plain of Soure is located on the Pará platform of northern Brazil. It pertains to a large area of crystalline and Palaeozoic sedimentary basement that remained tectonically stable relative to adjacent Cretaceous and Cenozoic sedimentary basins (Rossetti et al., 2008). The coastal plateau of northern Brazil is formed by the Barreiras Formation. These deposits occur from northern to southeastern Brazil and are of Miocene age (Arai, 1997).

Except for a narrow belt where the Barreiras Formation occurs, the eastern portion of the island is characterized by lowlands with altitudes averaging 4–6 m above the modern sea-level (Rossetti et al., 2007, 2008) and is dominated by Holocene sedimentation (Behling et al., 2004), which is topographically slightly lower than the western side (Behling et al., 2004; Rossetti et al., 2007; Lara and Cohen, 2009). Along the eastern portion, the Barreiras Formation is represented by sandstones and mudstones followed by post-Barreiras deposits (Rossetti et al., 2008).

Marajó Island has a river system consisting of numerous small, straight and meandering channels and ponds that are either permanent or ephemeral (Bemerguy, 1981). The flat surface of the eastern part of the island has been deeply incised by a drainage system during the Pleistocene and Holocene.

2.2. Present climate and vegetation

The region is characterized by a warm and humid tropical climate with annual precipitation averaging 2300 mm (Lima et al., 2005). The rainy season extends between December and May, with average temperatures ranging between 25 and 29 °C. The region is dominated by a regime of meso- and macrotides (tidal range of 2 to 4 m and 4 to 6 m, respectively) with variation during the spring tide between 3.6 and 4.7 m (DHN, 2003).

In contrast to most regions of Amazonia, where dense forest dominates, northeastern Marajó Island is covered with open vegetation. *Restinga* vegetation is represented by shrubs and herbs (e.g., *Anacardium*, *Byrsonima*, *Annona*, *Acacia*) that occur on sand plains and dunes near the shoreline. Mangrove is represented by *Rhizophora* and *Avicennia* (tree heights reaching ~20 m). The herbaceous plain consists of naturally open areas dominated by Cyperaceae and Poaceae that widely colonize the eastern side of Marajó Island. *Várzea* (swamp seasonally and permanently inundated by freshwater, featuring wetland trees such as *Euterpe oleracea* and *Hevea guianensis*) and Amazon coastal forest (ACF) (composed of terrestrial trees such as *Cedrela odorata*, *Hymenaea courbaril* and *Manilkara huberi*) occur on the western side (Cohen et al., 2008). Narrow and elongated belts of dense ombrophilous forest are also present along riverbanks (Rossetti et al., 2008). Detailed information on the most characteristic taxa of each vegetation unit is found in Smith et al. (2011).

3. Materials and methods

3.1. Field work and sample processing

LANDSAT images acquired in 2010 were obtained from INPE (National Space Research Institute, Brazil). A three-color band composition (RGB 543) image was created and processed using the SPRING 3.6.03 system to discriminate geobotanical units (Cohen and Lara, 2003). Aerial photography, visual observation, photographic documentation, and GPS measurements were used to determine typical plant species and characterize the main vegetation units.
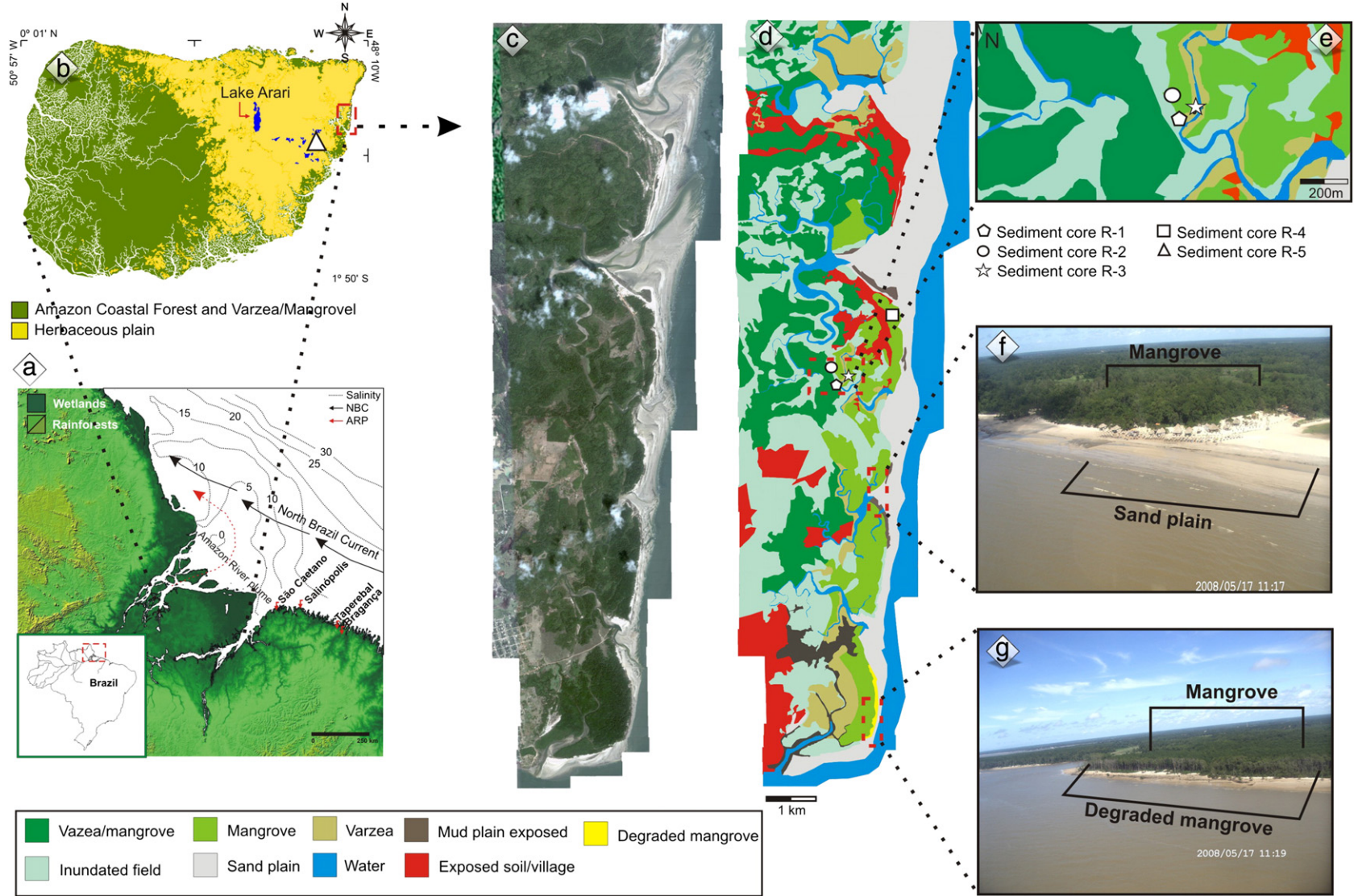
Fig. 1. Location of the study area: a) sea water salinity, Amazon River plume and North Brazil Current (Santos et al., 2008), b) Marajó Island; c) source coastal plain; d) vegetation units; e) sampling site on Soure coastal plain; f) mangrove and sand plain; g) degraded mangrove.

Table 1
Study site, vegetation types, sampling method and geographic coordinates in the coastal plain of Soure– eastern Marajó Island.

Cody site	Unit vegetation and main taxa	Sampling method	Coordinates
R-1	Mangrove/varzea transition — characterized by *Rhizophora mangle* and others taxa: Arecaceae (*Euterpe oleracea*; *Mauritia flexuosa*); Araceae (*Montrichardia arborescens*); Aizoaceae (*Sesuvium*); Acanthaceae (*Avicennia germinans*); Cyperaceae; Heliconiaceae; Musaceae; Myrtaceae (*Psidium guajava*); Poaceae (*Olyra*); Pteridaceae (*Acrostichum auereum*).	Russian sampler	S 00°40′ 26.3/ W 048°29′ 37.2″
R-2	Mangrove — characterized by *Rhizophora mangle*.	Russian sampler	S 00°40′ 23.1/ W 048°29′ 38.8″
R-3	Herbaceous and restinga vegetation — characterized by Arecaceae (*Euterpe oleracea*; *Mauritia flexuosa*); Birzonimia; Cyperaceae; Poaceae (*Olyra*); Malpiguiaceae.	Russian sampler	S 00°40′ 25.2″/ W 48°29′ 35.7″
R-4	Mangrove — characterized by *Rhizophora mangle*.	Vibracorer	S 00°39′ 37″/W 048°29′3.3″
R-5	Herbaceous flat — characterized by Convovulaceae; Rubiaceae; Cyperaceae and Poaceae.	Vibracorer	S 00°55′ 41″/W 048°39′47″

Three sediment cores (R-1, R-2 and R-3) were collected during the summer season (Nov. 2008), using a Russian sampler (Cohen, 2003), and two other cores were taken with a vibracorer using aluminum tubes (R-4 and R-5). Cores were taken from an area occupied by different vegetation units: mangroves (R4 and R2), *várzea* (R-1), mangrove and herbaceous vegetation (R-3), and a lacustrine herbaceous plain (R-5) (Table 1).

The cores were submitted to X-ray to identify sedimentary structures. Samples were collected for grain size analysis at the Chemical Oceanography Laboratory of the Federal University of Pará (UFPA). This analysis made use of a laser particle size analyzer (SHIMADZU SALD 2101), and graphics were obtained using the Sysgran Program (Camargo, 1999). Grain size distribution followed Wentworth (1922), with separation of sand (2–0.0625 mm), silt (62.5–3.9 μm) and clay (3.9–0.12 μm) fractions. Facies analysis included descriptions of color (Munsell Color, 2009), lithology, texture and structure (Harper 1984; Walker, 1992). The sedimentary facies were codified according to Miall (1978).

3.2. Pollen and spore analyses

For pollen analysis, 1 cm³ samples were taken at 2.5 cm intervals along sediment cores R-1, R-2 and R-3 (each 150 cm deep). From sediment cores R-4 and R-5, 24 and 36 samples were collected, respectively. Prior to processing, one tablet of exotic *Lycopodium* spores was added to each sediment sample to allow the calculation of pollen concentration (grains cm^{-3}) and pollen influx rates (grains cm^{-2} yr^{-1}). All samples were prepared using standard analytical techniques for pollen including acetolysis (Faegri and Iversen, 1989). Sample residues were placed in Eppendorf microtubes and kept in a glycerol gelatin medium. Reference morphological descriptions (Roubik and Moreno, 1991; Behling, 1993; Herrera and Urrego, 1996) were consulted for identification of pollen grains and spores. A minimum of 300 pollen grains were counted in each sample. The pollen sum excludes fern spores, algae and microforaminifers. Pollen and spore data are presented in diagrams as percentages of the pollen sum. Taxa were grouped into mangrove, herbaceous plain elements, *restinga*, palms, and Amazon coastal forest. Software packages TILIA and TILIAGRAF were used to calculate and plot pollen diagrams. The pollen diagrams were statistically subdivided into zones of pollen and spore assemblages using a square-root transformation of the percentage

data, followed by stratigraphically constrained cluster analysis (Grimm, 1987).

3.3. Radiocarbon dating

Based on stratigraphic discontinuities suggesting changes in the tidal inundation regime, fourteen bulk samples (10 g each) were selected. In order to avoid natural contamination (e.g. Goh, 2006), the sediment samples were checked and physically cleaned under the microscope. The organic matter was submitted to chemical treatment to remove any younger organic fractions (fulvic and/or humic acids) and carbonates. This treatment consisted of extracting residual material with 2% HCl at 60 °C during 4 h, washing with distilled water until neutral pH, followed by drying at 50 °C. A detailed description of the chemical treatment for sediment samples can be found in Pessenda and Camargo (1991) and Pessenda et al. (1996). A chronological framework for the sedimentary sequence was provided by conventional and accelerator mass spectrometer (AMS) radiocarbon dating. Samples were analyzed at the University of Georgia's Center for Applied Isotope Studies (UGAMS). Radiocarbon ages are reported as ^{14}C yr (1σ) BP normalized to a δ^{13}C of −25‰ VPDB and calibrated years as cal yr (2σ) BP using CALIB 6.0 (Stuiver et al., 1998; Reimer et al., 2004, 2009). In the text we use the median of the range for our and other authors' data.

4. Results

4.1. Radiocarbon dates and sedimentation rates

Radiocarbon dates for cores R-1 to R-5 are shown in Table 2. Sedimentation rates are between 0.1 and 10 mm yr^{-1} (Figs. 2 and 3). Although the rates are nonlinear between the dated points, they are within the vertical accretion range of 0.1 to 10 mm yr^{-1} of mangrove forests as reported by other authors (e.g. Bird, 1980; Spenceley, 1982 and Cahoon and Lynch, 1997; Behling et al., 2004; Cohen et al., 2005a, 2008, 2009; Vedel et al., 2006; Guimarães et al., 2010).

Table 2
Radiocarbon dates of sediment cores R1 to R5 and sample specific data.

Cody site	Laboratory number	Depth (cm)	Radiocarbon ages (yr BP)	CALIB age − 2σ (cal yr BP)	Median of age range (cal yr BP)	δ^{13}C (‰)
R-1	UGAMS4924	147–150	540 ± 25	560–520	540	−27.8
R-2	UGAMS4925	147–150	1260 ± 30	1160–1120	1140	−28.2
R-3	UGAMS4927	107–110	40 ± 25	70–30	50	−28.5
R-3	UGAMS4926	147–150	690 ± 25	680–640	660	−28.8
R-4	UGAMS4931	2–4	Modern	–	–	−29.3
R-4	UGAMS5316	44–46	Modern	–	–	−27.7
R-4	UGAMS5317	65–69	620 ± 25	620–560	590	−27.5
R-4	UGAMS4932	190–192	1530 ± 30	1520–1460	1490	−26.1
R-4	UGAMS5318	209–211	1510 ± 25	1420–1340	1380	−26.4
R-4	UGAMS4933	218–220	1760 ± 30	1740–1570	1655	−26.6
R-5	UGAMS4928	22–24	1920 ± 30	1950–1820	1885	−25.3
R-5	UGAMS8209	78–83	5730 ± 30	6640–6580	6610	−30.2
R-5	UGAMS4929	142–146	5840 ± 30	6740–6600	6670	−27.0
R-5	UGAMS5319	158–160	6750 ± 30	7670–7580	7625	−26.5
R-5	UGAMS8207	185–194	6150 ± 30	7160–6960	7060	−29.1
R-5	UGAMS8208	234–240	5860 ± 30	6780–6770	6775	−29.3
R-5	UGAMS4930	248–251	6600 ± 30	7530–7440	7485	−27.1

Fig. 2. Sediment profile with sedimentary features and ecological groups from cores R-1, R-2 and R-3.

Fig. 3. Sediment profile with sedimentary feature and ecological groups from cores R-4 and R-5.

4.2. Facies description and pollen association

The cores present dark gray and light brown muddy and sandy silt with an upward increase in grain size. These deposits are massive, parallel laminated or heterolithic-bedded. The texture and description of sedimentary structures allowed the identification of eleven sedimentary facies (Table 3).

A cluster analysis of pollen assemblages allowed the definition of pollen zones for each sediment core. The pollen diagrams show pollen types (Figs. 4, 5, 6, 7 and 8) and the proportions represented by the different ecological groups (Figs. 2 and 3). Pollen concentration and pollen influx values range from 5000 to 100,000 grains cm^{-3} and from 100 to 8000 grains cm^{-2} yr^{-1}, respectively.

The sediment and pollen analyses allowed the identification of five facies associations, described below.

4.3. Mangrove/herbaceous flat facies association

The mangrove/herbaceous flat occurs along the interval 150–135, 150–95 and 15–0 cm in R-1, R-2 and R-3, respectively (Fig. 2). This unit consists mostly of massive mud (facies Mm) with plant debris, and bioturbated coarse- to fine-grained sand (facies Sb).

The pollen assemblages of this association correspond to zone R1#1 (Fig. 4), R2#1 (Fig. 5) and R3#2 (Fig. 6). Zone R1#1 (560–520 cal yr BP until ~480 cal yr BP) is characterized by pollen of *Rhizophora* (15–65%), Cyperaceae (5–40%), Poaceae (2–30%), Fabaceae (2–20%), Mimosaceae (2–10%), *Borreria* (~5%), Rubiaceae (5–15%) and Amaranthaceae (2–7%). Zone R2#1 (1160–1120 cal yr BP until ~700 cal yr BP) is characterized by pollen of *Rhizophora* (10–75%), Cyperaceae (10–70%), Poaceae (5–20%), Fabaceae (2–10%) and Rubiaceae (1–5%). The presence of pollen from the Amazon coastal forest can be observed in this zone, represented by Euphorbiaceae (5–20%). Zone R3#2 (1993 AD until present) is characterized mainly by a decrease in *Rhizophora* (35–80%) and increase in Poaceae (10–25%) and Cyperaceae (5–15%) pollen.

4.4. Mangrove flat facies association

Cores R-1 and R-2 show the mangrove tidal flat along the intervals 135–0 and 95–0 cm, while this association occurs at depth interval 150–15 cm in R-3, 40–0 cm in R-4, and between 255 and 15 cm in R-5 (Figs. 2 and 3). The deposit consists of mud with flat lenses of rippled sand (facies Hl). Bioturbated mud (facies Mb), bioturbated sand (facies Sb), massive sand (facies Sm) and cross laminated fine-grained sand (facies Sc) are also present in this association. In addition, core R-1 displays mud with convolute lamination, which may contain roots, root channels and dwelling structures produced by benthic fauna.

The pollen assemblages of this association correspond to zone R1#2 (~480 cal yr BP — modern, Fig. 4), zone R2#2 (~700 cal yr BP — modern, Fig. 5) and to zone R3#1 (~660 cal yr BP — ~1993 AD, Fig. 6) in its entirety. This association also occurs in zone R4#3 (~600 cal yr BP — modern, Fig. 7), and zone R5#1 (~7500 cal yr BP — ~3200 cal yr BP, Fig. 8) and is characterized by the predominance of mangrove pollen, mainly represented by *Rhizophora* (40–95%). Pollen of herbaceous plain vegetation of the Cyperaceae, Poaceae, Fabaceae, Mimosaceae, *Borreria*, Rubiaceae, Amaranthaceae and Asteraceae occur at very low percentages (<30%).

4.5. Lagoon facies association

This association is mainly represented by massive mud (facies Mm) and massive sand (facies Sm), with mangrove pollen along zone R4#2 (70–40 cm). These deposits contain root and root marks, benthic tubes, mud and very fine silt to medium sand. The presence of mangrove is marked by *Rhizophora* (65–90%) and *Avicennia* (5%) pollen.

4.6. Foreshore facies association

This association occurs in core R-4 (225–70 cm), about >1650 to 580 cal yr BP, corresponding to zone R4#1. It consists of parallel-laminated, fine- to medium-grained sand (facies Sp). Roots, root marks

Table 3
Lithofacies description of cores R-1, R-2, R-3, R-4 and R-5 from the coastal plain of Soure, eastern margin of Marajó Island.

| Facies	Description	Sedimentary process
Bioturbated mud (Mb)	Brownish black and brown mud with many roots and root marks, dwelling structure and diffuse fine sand following the root traces and benthic tubes.	Diffused mixture of sediments and alternating colors by intense bioturbation and diagenic process.
Lenticular heterolitic (Hl)	Dark brown mud with single and connected flat lenses of bright brown, rippled fine to very fine sand.	Low energy flows with mud deposition from suspension, but with periodic sand inflows through migration of isolated ripples.
Cross laminated sand (Sc)	Brownish gray, well sorted, fine to medium sand with current ripple cross-lamination.	Migration of small ripples formed during low energy, either unidirectional or combined (unidirectional and oscillatory) flows.
Bioturbated sand (Sb)	Pale olive silty sand with light gray mottles, many roots, roots traces in growth position and dwelling structures.	Sediment homogenization and mottling by biological activity and diagenic process, respectively.
Parallel laminated mud (Mp)	Plastic, gray to black mud with parallel lamination and muds with thin, continuous streaks of gray to olive, silty to very fine grained sand.	Deposition of mud from suspension under very low flow energy.
Massive mud (Mm)	Plastic, massive mud, gray to dark gray and green, with many roots and root marks	The absence of structures in muddy indicates low flow energy during the sediment accumulation.
Mud/sand grains (Mms)	Gray and greenish gray, mud deposits with fine grained sand.	The absence of structures suggests the transported material by traction during the sediment deposition. This structure and the relative grain size increase may be produced by suspension or sedimentary dispersion through pulse of adjacent environmental and flow energy (tidal).
Massive sand (Sm)	Light yellow, moderately sorted, fine-grained massive sand. Mud intraclasts are either disperse or locally form conglomeratic lags.	The massive nature of these deposits might have been produced during drilling. Therefore, the most likely is that these deposits were, at least in great part stratified.
Parallel-laminated sand (Sp)	Fine-to-medium grained sand with parallel lamination or stratification. Local association with mud drape.	High (upper plane bed) energy flows. Parallel laminated sands with mud interbedding are related to low energy flows, before the stage of ripple development.
Heterolithic deposits wavy (Hw)	Greenish gray, mud layers interbedded with fine-to-medium-grained sand forming *wavy* structures.	Periods of mud and sand deposition from suspension and bed-load transport, respectively.
Flaser heterolithic deposit (Hf)	Gray mud layers interbedded with fine-to-medium-grained sand forming *flaser* structures.	Fluctuating low and relatively higher flow energies, with a balance between mud deposition from suspensions and sand deposition either from suspension or migrating ripples.
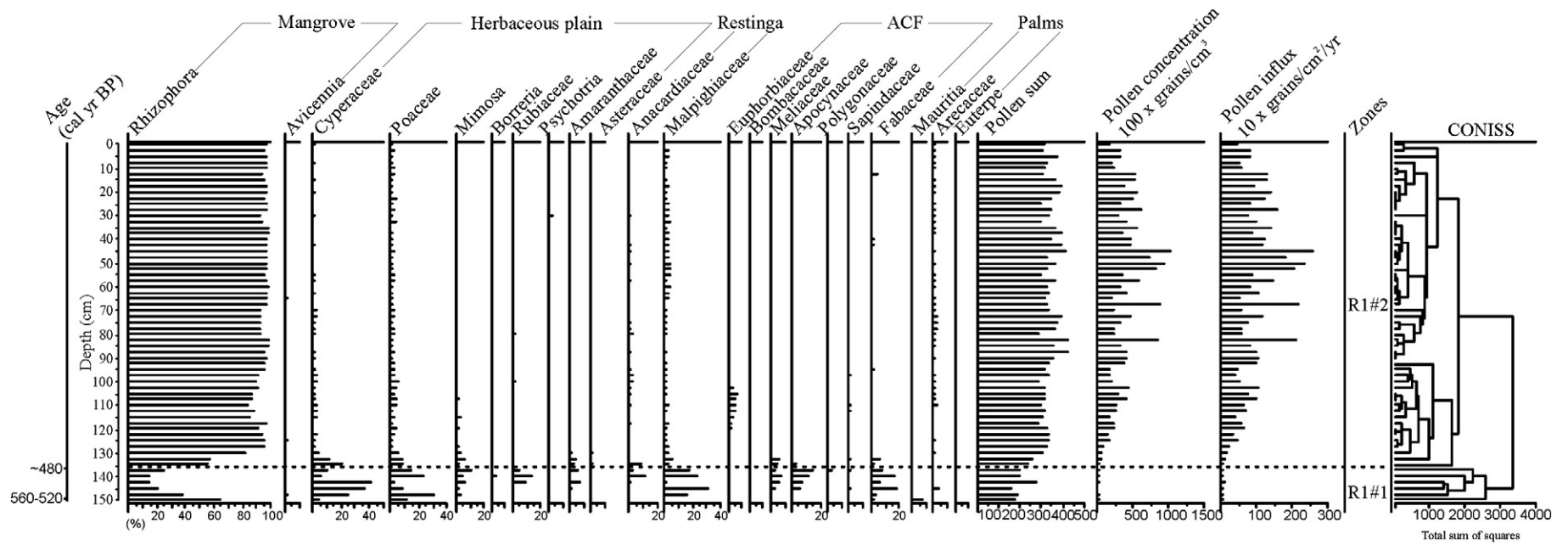
Fig. 4. Pollen record from core R-1 with percentages of the most frequent pollen taxa and sample age.
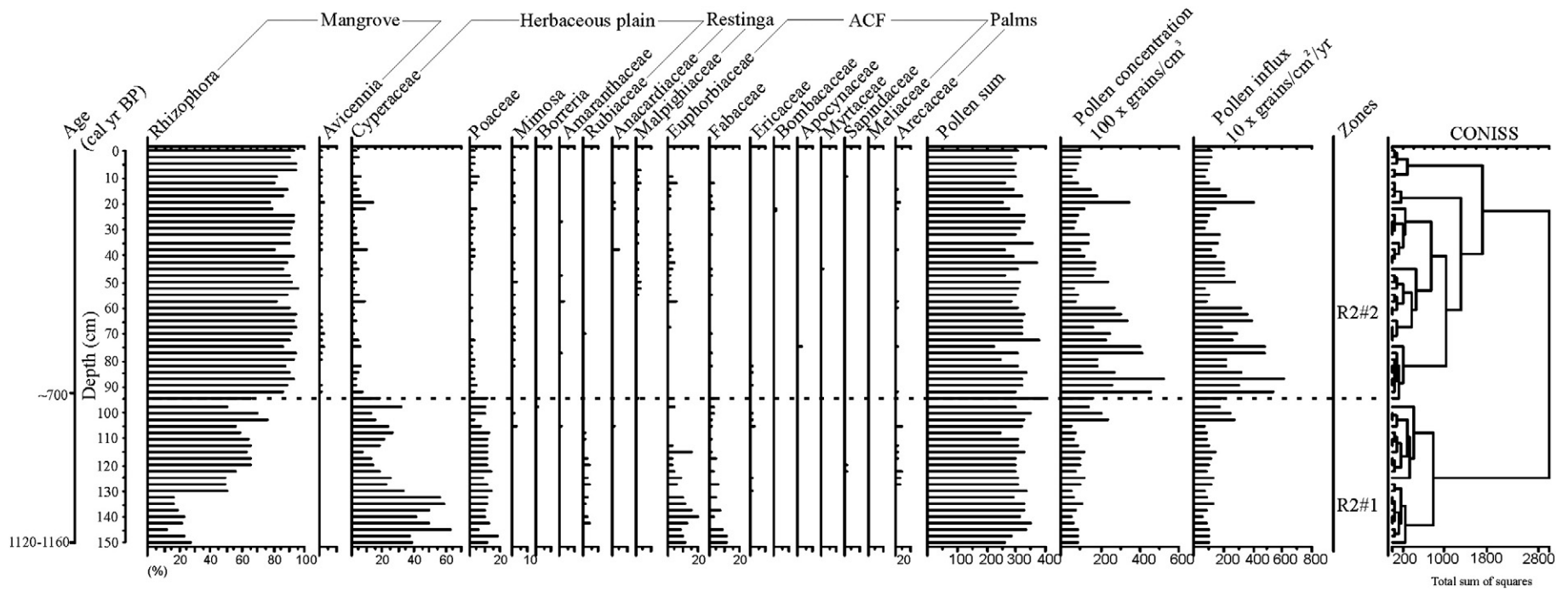
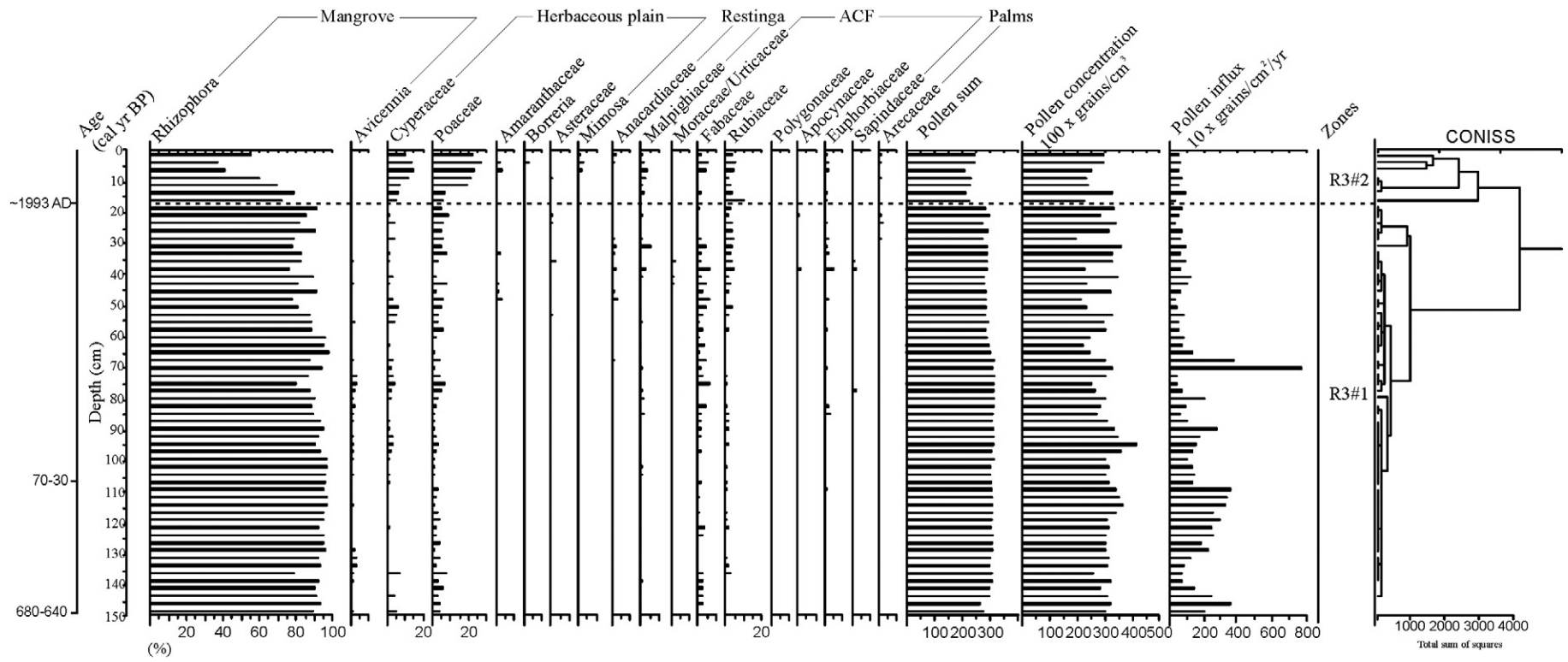Fig. 5. Pollen record from core R-2 with percentages of the most frequent pollen taxa and sample age.

Fig. 6. Pollen record from core R-3 with percentages of the most frequent pollen taxa and sample age.
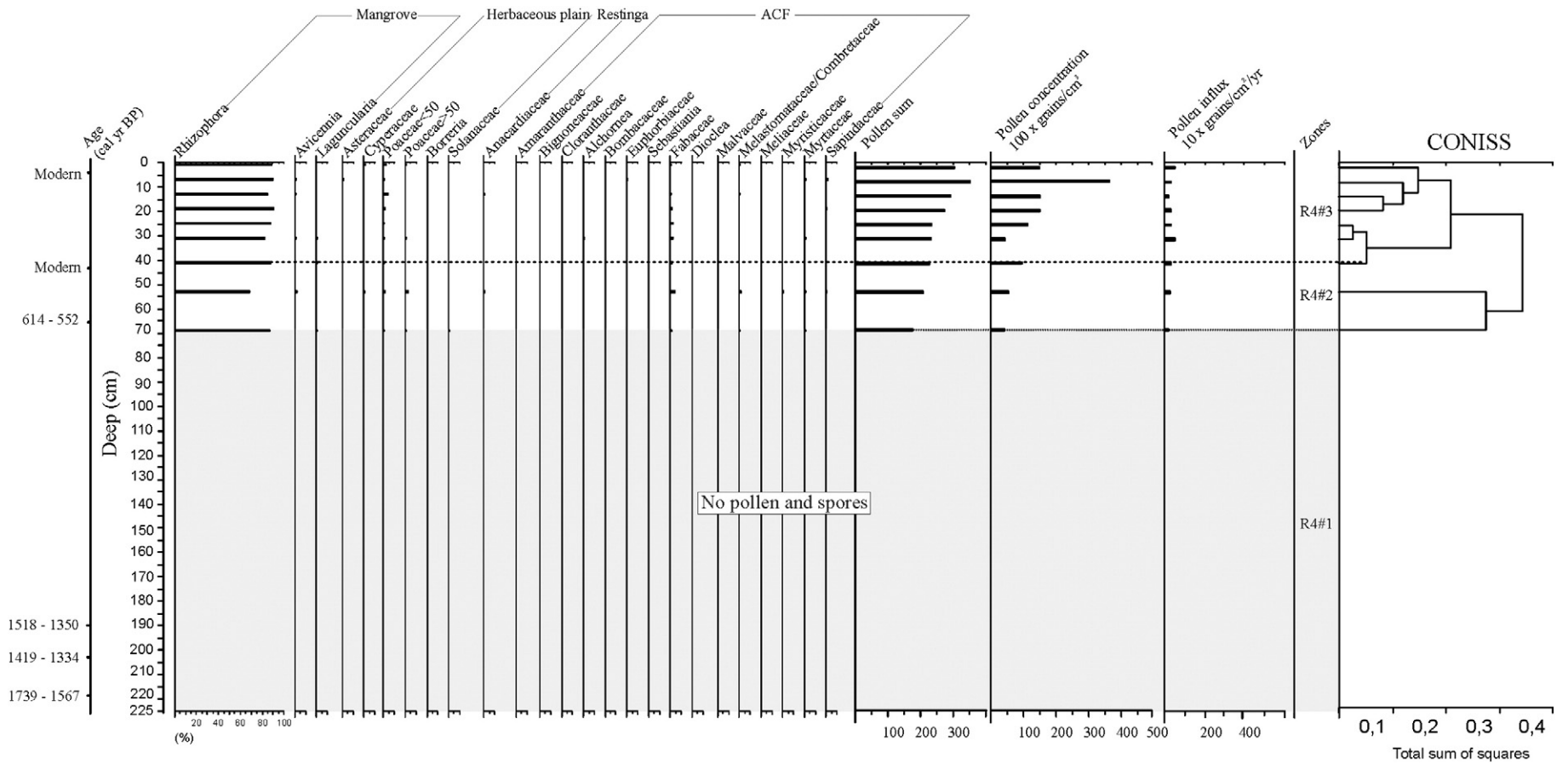
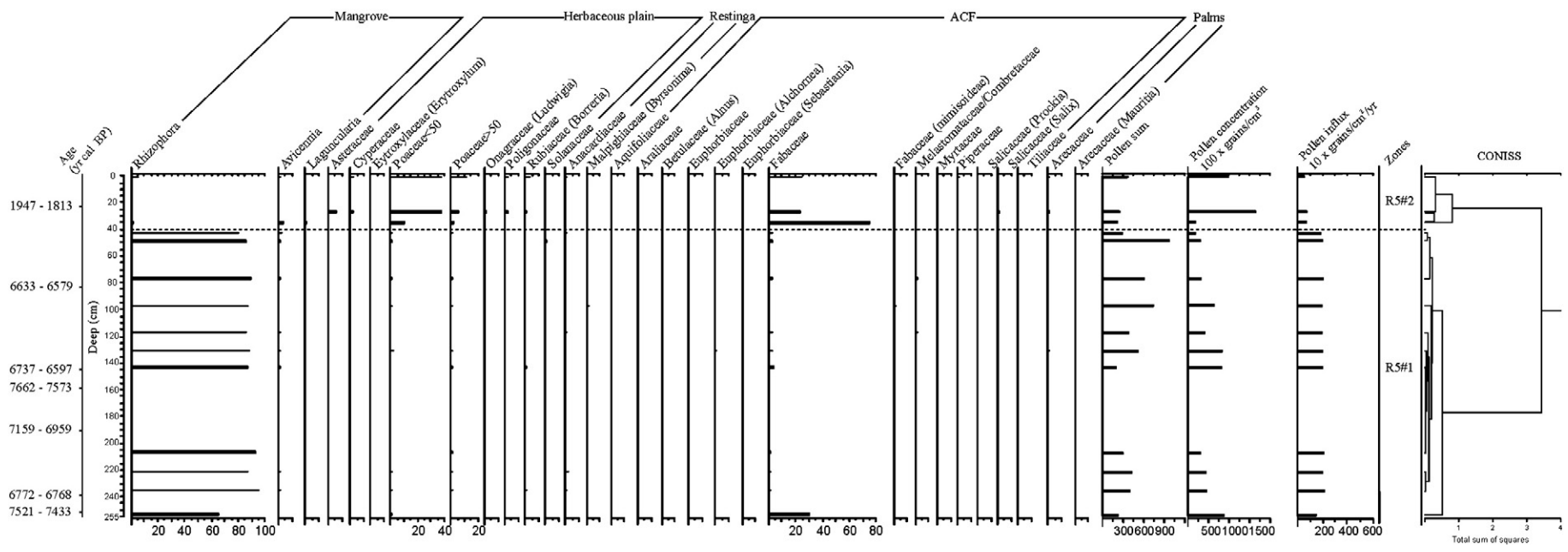**Fig. 7.** Pollen record from core R-4 with percentages of the most frequent pollen taxa and sample age.

Fig. 8. Pollen record from core R-5 with percentages of the most frequent pollen taxa and sample age.

and benthic tubes are present locally. Bedding is marked by heavy minerals and/or clay films (Fig. 3). The base is characterized by very fine- to medium-grained sand, and either heterolithic wavy deposits (facies Hw) and flaser heterolithic deposits (Hf). In addition, plant debris and oxidized iron blades are present. These deposits did not contain pollen grains.

4.7. Lake facies association

This association occurs only in core R-5 (R5#2), between 55 and 0 cm (Figs. 3 and 8). It is characterized by massive mud (facies Mm) and bioturbated mud (Mb). Benthic tubes, oxidized iron concretions, plant debris and root marks were present. These deposits are marked by greater amounts of pollen which is characteristics of ACF (3–75%), herbs (2–55%), aquatic vegetation (0–10%) and ferns (1–5%), and accompanied by a decrease in mangrove pollen (85–0%).

5. Discussion

5.1. Pollen signal and vegetation changes in Marajó Island during the Holocene (central and eastern coastal zone)

There often exists two pollen components in sediment—pollen from "local" vegetation, and background pollen from "regional" vegetation (Janssen 1966, 1973; Andersen 1967; Sugita 1994). Pollen records of lacustrine sediment cores include pollen sourced from vegetation surrounding the lake, considering that winds blow from various directions. Thus, the proportion of the pollen signal provided by each vegetation type is distance-weighted (e.g. Davis, 2000). Some empirical studies have reported pollen transport in rivers (e.g. Brush and Brush, 1972; Solomon et al., 1982). Flume experiments suggest that pollen grains will settle out into sediment when water velocity is lower than 0.3 m s^{-1}, and therefore grains can remain in suspension and be transported to long distances when water velocity is greater than 0.3 m s^{-1} (Brush and Brush, 1972). According to Xu et al. (2012), the pollen found in lakes originates from three components: an aerial component mainly carried by wind, a fluvial catchment component transported by rivers and a third waterborne component transported by surface wash. Overall, vegetational composition within the 'aerial catchment' differs from that of the hydrological catchment.

Influx rates of modern pollen from the Bragança Peninsula, located 150 km east of the study area, indicate that *Rhizophora* is a very prolific pollen producer within mangroves, while *Avicennia* and *Laguncularia* produce lesser amounts. Pollen influx rates of *Rhizophora* and *Avicennia* in the *Rhizophora/Avicennia* dominated forest area are approximately 14,500 and 450 grains $\text{cm}^{-2}\text{ yr}^{-1}$, respectively. Pollen traps in the herbaceous plain site, which are located at least 1–2 km away from the nearest *Rhizophora* trees and 100 m away from the nearest *Avicennia*, document an average of 410 *Rhizophora* grains $\text{cm}^{-2}\text{ yr}^{-1}$ and an average of 8 *Avicennia* grains $\text{cm}^{-2}\text{ yr}^{-1}$. This indicates that a certain amount of *Rhizophora* pollen grains can be transported by wind, while wind transportation of *Avicennia* pollen is very low (Behling et al., 2001).

Core R-5, sampled from a lake and currently dominated by herbaceous vegetation (Fig. 1), indicates change in vegetation patterns. This change likely extends at least to the drainage basin area and is expected to be reflected in pollen records of the lacustrine sediments. Pollen contributions from different vegetation type in the surrounding landscape are also expected to decrease with increasing distance from the lake. For this reason the pollen record of core R-5, at least between depths of 0 and 55 cm, is likely more representative of vegetation dynamics of eastern Marajó Island than those records from cores R-1, R-1, R-3 and R-4, collected from tidal flats.

The results obtained from pollen and sedimentological analyses suggest vegetation changes during the last seven thousand years. The sedimentary deposits consisting of mud/sand alternations formed under oscillating flow energy contain three pollen groups. Vegetation shifts

most likely occurred under the influence of fluctuating flow velocity asymmetry in tidal flats. Data suggest a tidal mud flat colonized by mangroves in the central region of the island between ~7500 cal yr BP and ~3200 cal yr BP, as recorded in core R-5 (Figs. 3 and 8), and other cores from Lake Arari on Marajó Island during the early and mid Holocene (Smith et al., 2011, 2012).

During the late Holocene in the hinterland of Marajó Island, mangroves were largely replaced by herbaceous vegetation. Mangroves occurred on tidal flats on the northeastern coast of the island (i.e., core R-2) at least since ~1150 cal yr BP, and continued to be recorded in cores R-1, R-4 and R-3 at 540, 580 and 660 cal yr BP, respectively.

The migration of mangroves recorded in core R-4 (Fig. 7) may be a natural response to coast progradation, following stabilization and mud accumulation. Progradation could have also affected other areas of the Marajó coastline, where *várzea* became established instead of mangrove (Cohen et al., 2008 and Smith et al., 2011).

Therefore, mangrove vegetation at the mouth of the Amazon River retreated to a narrow area of northeastern Marajo Island. An increment in river discharge near Marajó Island during the late Holocene constitutes a hypothesis for this isolation (Guimarães et al., 2012; Smith et al., 2012). This process could be responsible for the modern decrease in tidal water salinity along the littoral (0–6‰, Santos et al., 2008). It is noteworthy that tidal water salinity is greater in this northeastern area than elsewhere on the island, and this is related to the southeast–northwest trending current along the littoral. This current displaces brackish waters from the marine influenced littoral (Fig. 1a).

Greater tidal water salinity during the early and mid Holocene could be attributed to the episode of Atlantic sea-level rise recorded in other parts of South America (e.g., Suguio et al., 1985; Tomazelli, 1990; Rull et al., 1999; Hesp et al., 2007; Angulo et al., 2008). This event could have also produced a marine incursion along the Pará littoral, where the RSL stabilized at its current level between 7000 and 5000 yr BP (e.g. Cohen et al., 2005b; Vedel et al., 2006). A transgressive phase occurred on Marajó Island in the early to mid-late Holocene. Subsequently, there was a return to the more continental conditions that prevail today in the study area (Rossetti et al., 2008). This history of RSL fluctuations on Marajó Island seems to have been affected by tectonic activity during the Late Pleistocene and Holocene (Rossetti et al., 2008; Rossetti, et al., 2012). Hence, transgression was favored during increased subsidence, when space was created to accommodate new sediments. Tectonic stability seems to have prevailed during the mid to late Holocene, leading to coastal progradation that culminated with more continental conditions prevailing on the island.

The post-glacial sea-level rise, likely combined with tectonic subsidence, caused a marine transgression. The tidal water salinity should have further increased due to low river discharge resulting from increased aridity during the early and mid Holocene. If river systems are considered to be integrators of rainfall over large areas (Amarasekera et al., 1997), variations in the discharge of the Amazon River during the Holocene may be a consequence of changes in rainfall rates, as recorded in many different regions of the Amazon Basin (e.g. Bush and Colinvaux, 1988; Absy et al., 1991; Sifeddine et al., 1994; Desjardins et al., 1996; Gouveia et al., 1997; Pessenda et al., 1998a, 1998b, 2001; Behling and Hooghiemstra, 2000; Freitas et al., 2001; Sifeddine et al. 2001; Weng et al., 2002; Bush et al., 2007; Guimarães et al., 2012).

5.2. Mangrove dynamics during the last decades in the eastern coastal zone of Marajó Island

Mangroves preferentially occupy mudflats. Mangrove retreat along the coastline may be caused by landward sand migration, which covers the mudflat and asphyxiates the vegetation (Cohen and Lara, 2003). During the last one hundred years, the increase inflow energy on mangroves (Furukawa and Wolanski, 1996) evidenced at Marajó Island by the upward mud into sand (Figs. 1f and 1g) may also contribute to mangrove retraction, as recorded in the upper section of core R-3 (Fig. 6).

The disappearance of mangrove vegetation along the Marajó coastline has been mostly caused by erosion and landward sand migration above mangrove mud sediments (Fig. 1g). At present, this region is exposed to wave action and tidal currents in Marajó Bay, which apparently have caused the retreat of the coastline, and consequently a reduction in the area covered by mangrove vegetation.

This process is also evidenced along the Pará littoral. The marine influenced littoral in the central area of peninsulas also shows a transition between herbaceous vegetation and mangrove forest, with mangrove migration toward the topographically highest herbaceous areas most likely in response to the modern RSL rise (Cohen and Lara 2003; Cohen et al., 2009).

Greater exposure to tidal influence may have been driven by RSL rise and/or by greater river water discharge. As previously mentioned, the RSL rise in this area may be related to tectonics and it may reduce areas favorable for mangrove development (Blasco et al. 1996) leading to the migration of this ecosystem to topographically more elevated terrains (Cohen and Lara, 2003; Cohen et al. 2005a).

Climate fluctuations (Molodkov and Bolikhovskaya, 2002) which impacted rainfall (e.g. Absy et al. 1991; Pessenda et al., 1998a,b, 2001, 2004; Behling and Costa, 2000; Freitas, et al., 2001; Maslin and Burns, 2001) could also have caused changes in river flow and estuarine salinity gradients (Lara and Cohen, 2006). This can also affect the RSL (Mörner, 1996).

The area covered by herbaceous vegetation, located in topographically higher areas, suffered a reduction during the last decades (Cohen and Lara, 2003) and centuries (Cohen et al., 2005a). This indicates an increase in the RSL, which has caused erosion and deposition of sand over mud deposits. This trend was also observed on the Taperebal (12 km north of Bragança) (Vedel et al., 2006). The effects of RSL rise were also observed in cores taken from São Caetano de Odivelas and Salinópolis (Cohen et al., 2009) in the northeastern coast of Pará, in the eastern Amazon region.

6. Conclusions

The integration of pollen data and facies descriptions of five sediment cores indicates a tidal mud flat colonized by mangroves in the interior of Marajó Island between ~7500 cal yr BP and ~3200 cal yr BP. During the late Holocene, mangroves became isolated and grew on a small area (100–700 m width) of the northeastern part of the island. This likely results from lower tidal water salinity caused by a wet period that resulted in greater river discharge during the late Holocene. The northeastern area of the island exhibits relatively greater tidal water salinity, due to the southeast–northwest trending littoral current which brings brackish waters from more marine influenced areas. It has provided a refuge for the mangroves of Marajó Island.

Over the last century, the increase in flow energy evidenced by upward mud/sand transitions also contributes to mangrove retraction, as recorded in the upper part of core R-3. This is mainly due to landward sand migration, which covers the mudflat and asphyxiates the mangrove. The increase in flow energy and exposure to tidal influence may have been driven by the RSL rise, either associated with global fluctuations or tectonic subsidence, and/or by the increase in river water discharge. These processes can modify the size of the area occupied by mangroves.

As demonstrated by this work, using a combination of proxies is efficient for palaeoenvironmental reconstruction, where mangrove retraction during the late Holocene shows the high degree of sensitivity of this ecosystem to the sequence of environmental variables discussed here.

Acknowledgments

References

Absy, M.L., Cleef, A., Fournier, M., Martin, L., Servant, M., Sifeddine, A., Ferreira da Silva, M., Soubies, F., Suguio, K., Turcq, B., Van Der Hammen, T.H., 1991. Mise en evidence de quatre phases d'overture de la forêt dense dans le sud-est de l'Amazonie au cours des 60,000 dernieres annees. Premiere comparision avec d'autres regions tropicales. Comptes Rendus de l'Académie des Sciences 312, 673–678.

Alongi, D.M., 2008. Mangrove forests: resilience, protection from tsunamis, and responses to global climate change. Estuarine, Coastal and Shelf Science 76, 1–13.

Alongi, D.M., Sasekumar, A., Tirendi, F., Dixon, P., 1998. The influence of stand age on benthic decomposition and recycling of organic matter in managed mangrove forests of Malaysia. Journal of Experimental Marine Biology and Ecology 225, 197–218.

Alongi, D.M., Tirendi, F., Dixon, P., Trott, L.A., Brunskill, G.J., 1999. Mineralization of organic matter in intertidal sediments of a tropical semi-enclosed delta. Estuarine, Coastal and Shelf Science 48, 451–467.

Alongi, D.M., Tirendi, F., Clough, B.F., 2000. Below-ground decomposition of organic matter in forests of the mangrove Rhizophora stylosa and Avicennia marina along the arid coast of Western Australia. Aquatic Botany 68, 97–122.

Amarasekera, K.N., Lee, R.F., Williams, E.R., Eltahir, E.A.B., 1997. ENSO and the natural variability in the flow of tropical rivers. Journal of Hydrology 200, 24–39.

Andersen, S.T., 1967. Tree-pollen rain in a mixed deciduous forest in south Jutland (Denmark). Review of Palaeobotany and Palynology 3, 267–275.

Angulo, R.J., de Souza, M.C., Assine, M.L., Pessenda, L.C.R., Disaró, S.T., 2008. Chronostratigraphy and radiocarbon age inversion in the Holocene regressive barrier of Paraná, southern Brazil. Marine Geology 252, 111–119.

Arai, M., 1997. Dinoflagelados (Dynophiceae) miocênicos do Grupo Barreiras do nordeste do estado do Pará (Brasil). Revista da Universidade de Guarulhos 2, 98–106.

Baltzer, F., 1970. Etude sédimentologique du marais de Mara (Côte ouest de la Nouvelle Calédonie) et de formations quaternaires voisines. Mémoires expédition française sur lês récifs coralliens de la Nouvelle Calédonie, 4. Foundation Singer-Polignac, pp. 146–169.

Baltzer, F., 1975. Solution of silica and formation of quartz and smectite in mangrove swamps and adjacent hypersaline marsh environments. Proceedings of the International Symposium on Biology and Management of Mangroves. University of Florida, Orlando, Florida, pp. 482–498.

Behling, H., 1993. Untersuchungen zur Spätpleistozänen und Holozänen Vegetations und Klimageschichte der Tropischen Küstenwälder und der Araukarienwälder in Santa Catarina (Südbrasilien). Dissertationes Botanicae, Berlin, Deutschland.

Behling, H., Costa, M.L., 2000. Holocene environmental changes from the Rio Curuá record in the Caxiuanã Region, eastern Amazon Basin. Quaternary Research 53, 369–377.

Behling, H., Hooghiemstra, H., 2000. Holocene Amazon rainforest–savanna dynamics and climatic implications: high-resolution pollen record from Laguna Loma Linda in eastern Colombia. Journal of Quaternary Science 15, 687–695.

Behling, H., Cohen, M.C.L, Lara, R.J., 2001. Studies on Holocene mangrove ecosystem dynamics of the Bragança Peninsula in north-eastern Pará, Brazil. Palaeogeography, Palaeoclimatology, Palaeoecology 167, 225–242.

Behling, H., Cohen, M.C.L., Lara, R.J., 2004. Late Holocene mangrove dynamics of the Marajó Island in northern Brazil. Vegetation History and Archaeobotany 13, 73–80.

Bemerguy, R.L., 1981. Estudo sedimentológico dos paleocanais da região do Rio Paracauari, Ilha do Marajó – Estado do Pará. Dissertação de Mestrado, Universidade Federal do Pará, Belém, Brasil.

Berger, U., Rivera-Monroy, V.H., Doyle, T.W., Dahdouh-Guebas, F., Duke, N.C., Fontalvo-Herazo, M.L., Hildenbrandt, H., Koedam, N., Mehlig, U., Piou, C., Twilley, R., 2008. Advances and limitations of individual-based models to analyze and predict dynamics of mangrove forests: a review. Aquatic Botany 89, 260–274.

Bird, E.C.F., 1980. Mangroves and coastal morphology. The Victorian Nauralist 97, 48–58.

Blasco, F., Saenger, P., Janodet, E., 1996. Mangrove as indicators of coastal change. Catena 27, 167–178.

Brush, G.S., Brush, L.M.J., 1972. Transport of pollen in a sediment laden channel: a laboratory study. American Journal of Science 272, 359–381.

Bush, M.B., Colinvaux, P.A., 1988. A 7000-year pollen record from the Amazon lowlands, Ecuador. Vegetatio 76, 141–154.

Bush, M.B., Silman, M.R., Listopad, C.M.C.S., 2007. A regional study of Holocene climate change and human occupation in Peruvian Amazonia. Journal of Biogeography 34, 1342–1356.

Cahoon, D.R., Lynch, J.C., 1997. Vertical accretion and shallow subsidence in a mangrove forest of southwestern Florida, U.S.A. Mangroves and Salt Marshes 3, 173–186.

Camargo, M.G., 1999. SYSGRAN for Windows: Granulometric Analyses System. Pontal do Sul, Paraná, Brazil.

Chapman, V.J., 1976. Mangrove Vegetation. Velag Von J. Cramer, Leutershausen, Germany . p. 447.

Clark, M.W., McConchie, D.M., Lewis, D.W., Saenger, P., 1998. Redox stratification and heavy metal partitioning in Avicennia-dominated mangrove sediments: a geochemical model. Chemical Geology 149, 147–171.

Cohen, M.C.L., 2003. Past and current mangrove dynamics on the Bragança Península, northern Brazil. Ph.D. Thesis, University of Bremen, Center for Tropical Marine Ecology, Bremen, Germany.

Cohen, M.C.L., Lara, R.J., 2003. Temporal changes of mangrove vegetation boundaries in Amazonia: application of GIS and remote sensing techniques. Wetlands Ecology and Management 11, 223–231.

Cohen, M.C.L., Behling, H., Lara, R.J., 2005a. Amazonian mangrove dynamics during the last millennium: the relative sea-level and the Little Ice Age. Review of Palaeobotany and Palynology 136, 93–108.

Cohen, M.C.L., Souza Filho, P.W., Lara, R.L., Behling, H., Angulo, R., 2005b. A model of Holocene mangrove development and relative sea-level changes on the Bragança Peninsula (northern Brazil). Wetlands Ecology and Management 13, 433–443.

Cohen, M.C.L., Lara, R.J., Smith, C.B., Angélica, R.S., Dias, B.S., Pequeno, T., 2008. Wetland dynamics of Marajó Island, northern Brazil, during the last 1000 years. Catena 76, 70–77.

Cohen, M.C.L., Lara, R.J., Smith, C.B., Matos, H.R.S., Vedel, V., 2009. Impact of sea-level and climatic changes on the Amazon coastal wetlands during the late Holocene. Vegetation History and Archaeobotany 18, 425–439.

Cohen, M.C.L., Pessenda, L.C.R., Behling, H., Rossetti, D.F., França, M.C., Guimarães, J.T.F., Friaes, Y.S., Smith, C.B., 2012. Holocene palaeoenvironmental history of the Amazonian mangrove belt. Quaternary Science Reviews 55, 50–58.

Color, Munsell, 2009. Munsell Soil Color Charts, New Revised Edition. Macbeth Division of Kollmorgen Instruments, New Windsor, NY.

Davis, M.B., 2000. Palynology after Y2K—understanding the source area of pollen in sediments. Annual Review Earth Planetary Science 28, 1–18.

Departamento de Hidrografia e Navegação (DHN), Marinha do Brasil, 2003. Rio de Janeiro, Brasil.

Desjardins, T., Filho, A.C., Mariotti, A., Chauvel, A., Girardin, C., 1996. Changes of the forestsavanna boundary in Brazilian Amazonia during the Holocene as revealed by soil organic carbon isotope ratios. Oecologia 108, 749–756.

Faegri, K., Iversen, J., 1989. Textbook of Pollen Analysis, 4th. John Wiley and Sons, Chichester . p 328.

França, C.F., Sousa Filho, P.W.M., 2006. Compartimentação morfológica da margem leste da ilha de Marajó: zona costeira dos municípios de Soure e Salvaterra – Estado do Pará. Revista Brasileira de Geomorfologia 1, 33–42.

Freitas, H.A., Pessenda, L.C.R., Aravena, R., Gouveia, S.E.M., Ribeiro, A.S., Boulet, R., 2001. Late Quaternary vegetation dynamics in the southern Amazon basin inferred from carbon isotopes in soil organic matter. Quaternary Research 55, 39–46.

Fromard, F., Vega, C., Proisy, C., 2004. Half a century of dynamic coastal change affecting mangrove shorelines of French Guiana. A case study based on remote sensing data analyses and field surveys. Marine Geology 208, 265–280.

Furukawa, K., Wolanski, E., 1996. Sedimentation in mangrove forests. Mangroves and Salt Marshes 1, 3–10.

Gilman, E.L., Ellison, J., Duke, N.C., Field, C., 2008. Threats to mangroves from climate change and adaptation options: a review. Aquatic Botany 89, 237–250.

Goh, K.M., 2006. Removal of contaminants to improve the reliability of Radiocarbon dates of peats. Journal of Soil Science 29, 340–349.

Gonçalves-Alvim, S.J., Vaz dos Santos, M.C.F., Fernandes, G.W., 2001. Leaf gall abundance on *Avicennia germinans* (Avicenniaceae) along an interstitial salinity gradient. Biotropica 33, 69–77.

Gornitz, V., 1991. Global coastal hazards from future sea level rise. Palaeogeography, Palaeoclimatology, Palaeoecology 89, 379–398.

Gouveia, S.E.M., Pessenda, L.C.R., Aravena, R., Boulet, R., Roveratti, R., Gomes, B.M., 1997. Dinâmica de vegetações durante o Quaternário recente no sul do Amazonas indicada pelos isótopos do carbono (^{12}C, ^{13}C e ^{14}C). Geochimica Brasiliensis 11, 355–367.

Grimm, E.C., 1987. Coniss: a Fortran 77 program for stratigraphically constrained cluster analysis by the method of the incremental sum of squares. Computers & Geosciences 13, 13–35.

Guimarães, J.T.F., Cohen, M.C.L., França, M.C., Lara, R.J., Behling, H., 2010. Model of wetland development of the Amapá coast during the late Holocene. Anais da Academia Brasileira de Ciências 82, 451–465.

Guimarães, J.T.F., Cohen, M.C.L., Pessenda, L.C.R., França, M.C., Smith, C.B., Nogueira, A.C.R., 2012. Mid- and late-Holocene sedimentary process and palaeovegetation changes near the mouth of the Amazon River. The Holocene 22, 359–370.

Harper, C.W., 1984. Improved methods of facies sequence analysis, In: Walker, R.G. (Ed.), Facies Models, 2 ed. Geological Association of Canada, Ontario, Canada, pp. 11–13.

Herrera, L.F., Urrego, L.E., 1996. Atlas de polen de plantas útiles y cultivadas de la Amazonia colombiana (Pollen atlas of useful and cultivated plants in the Colombian Amazon region). Estudios en la Amazonia Colombiana, XI. Tropenbos-Colombia, Bogotá . p. 462.

Hesp, P.A., Dillenburg, S.R., Barboza, E.G., Clerot, L.C.P., Tomazelli, L.J., Zouain, R.N.A., 2007. Morphology of the Itapeva to Tramandai transgressive dunefield barrier system and midto late Holocene sea level change. Earth Surface Process and Landforms 32, 407–414.

Hesse, P.R., 1961. Some differences between the soils of *Rhizophora* and *Avicennia* mangrove swamp in Sierra Leone. Plant and Soil 14, 335–346.

Hutchings, P., Saenger, P., 1987. Ecology of Mangroves. Queensland University Press, St. Lucia, Qld., Australia and New York, p. 370.

Janssen, C.R., 1966. Recent pollen spectra from the deciduous and coniferous deciduous forests of northeastern Minnesota: a study in pollen dispersal. Ecology 47, 804–825.

Janssen, C.R., 1973. Local and regional pollen deposition. In: Birks, H.J.B., West, R.G. (Eds.), Quaternary Plant Ecology. Blackwell, Oxford, UK, pp. 31–42.

Lacerda, L.D., Ittekkot, V., Patchineelam, S.R., 1995. Biogeochemistry of mangrove soil organic matter: a comparison between *Rhizophora*, *Avicennia* soils in southeastern Brazil. Estuarine, Coastal and Shelf Science 40, 713–720.

Lamb, A.L., Wilson, G.P., Leng, M.J., 2006. A review of coastal palaeoclimate and relative sea-level reconstructions using δ^{13}C and C/N ratios in organic material. Earth-Science Reviews 75, 29–57.

Lara, J.R., Cohen, M.C.L., 2006. Sediment porewater salinity, inundation frequency and mangrove vegetation height in Bragança, North Brazil: an ecohydrology-based empirical model. Wetlands Ecology and Management 4, 349–358.

Lara, R.J., Cohen, M.C.L., 2009. Palaeolimnological studies and ancient maps confirm secular climate fluctuations in Amazonia. Climatic Change 94, 399–408.

Lima, A.M.M., Oliveira, L.L., Fontinhas, R.L., Lima, R.J.S., 2005. Ilha de Marajó: revisão histórica, hidroclimatológica, bacias hidrográficas e propostas de gestão. Holos Environment 5, 65–80.

Maslin, M., Burns, S.J., 2001. Reconstruction of the Amazon basin effective moisture availability over the past 14,000 years. Science 290, 2285–2287.

Matthijs, S., Tack, J., van Speybroeck, D., Koedam, N., 1999. Mangrove species zonation and soil redox state, sulphide concentration and salinity in Gazi Bay (Kenya), a preliminary study. Mangroves and Salt Marshes 3, 243–249.

McKee, K.L., 1995. Seedlings recruitment patterns in a Belizean mangrove forest: effects of establishment ability and physico-chemical factors. Oecologia 101, 448–460.

Menezes, M., Berger, U., Worbes, M., 2003. Annual growth rings and long-term growth patterns of mangrove trees from the Bragança peninsula, North Brazil. Wetlands Ecology and Management 1, 33–242.

Miall, A.D., 1978. Facies types and vertical profile models in braided river deposits: a summary. In: Miall, A.D. (Ed.), Fluvial Sedimentology. Canadian Society of Petroleum Geologists, Calgary, pp. 597–604.

Miranda, M.C.C., Rossetti, D.F., Pessenda, L.C.R., 2009. Quaternary paleoenvironments and relative sea-level changes in Marajó Island (Northern Brazil): Facies, δ^{13}C, δ^{15}N and C/N. Palaeogeography, Palaeoclimatology, Palaeoecology 282, 19–31.

Molodkov, A.N., Bolikhovskaya, N.S., 2002. Eustatic sea-level and climate changes over the last 600 ka as derived from mollusk based ERS-chronostratigraphy and pollen evidence in Northern Eurasia. Sedimentary Geology 150, 185–201.

Mörner, N.A., 1996. Global change and interaction of earth rotation, ocean circulation and paleoclimate. Anais da Academia Brasileira de Ciências 68, 77–94.

Pessenda, L.C.R., Camargo, P.B., 1991. Datação radiocarbônica de amostras de interesse arqueológico e geológico por espectrometria de cintilação líquida de baixo nível de radiação de fundo. Química Nova 14, 98–103.

Pessenda, L.C.R., Valencia, E.P.E., Martinelli, L.A., 1996. ^{14}C measurements in tropical soil developed on basic rocks. Radiocarbon 38, 203–208.

Pessenda, L.C.R., Gomes, B.M., Aravena, R., Ribeiro, A.S., Boulet, R., Gouveia, S.E.M., 1998a. The carbon isotope record in soils along a forest-cerrado ecosystem transect: implications for vegetation changes in the Rondonia state, southwestern Brazilian Amazon region. The Holocene 8, 631–635.

Pessenda, L.C.R., Gouveia, S.E.M., Aravena, R., Gomes, B.M., Boulet, R., Ribeiro, A.S., 1998b. ^{14}C dating and stable carbon isotopes of soil organic matter in forest savanna boundary areas in the southern Brazilian Amazon region. Radiocarbon 40, 1013–1022.

Pessenda, L.C.R., Boulet, R., Aravena, R., Rosolen, V., Gouveia, S.E.M., Ribeiro, A.S., Lamotte, M., 2001. Origin and dynamics of soil organic matter and vegetation changes during the Holocene in a forest-savanna transition zone, Brazilian Amazon region. The Holocene 11, 250–254.

Pessenda, L.C.R., Ribeiro, A.S., Gouveia, S.E.M., Aravena, R., Boulet, R., Bendassoli, J.A., 2004. Vegetation dynamics during the late Pleistocene in the Barreirinhas region, Maranhão State, northeastern Brazil, based on carbon isotopes in soil organic matter. Quaternary Research 62, 183–193.

Pezeshki, S.R., DeLaune, R.D., Meeder, J.F., 1997. Carbon assimilation and biomass in *Avicennia germinans* and *Rhizophora mangle* seedlings in response to soil redox conditions. Environmental and Experimental Botany 37, 161–171.

Reimer, P.J., Baillie, M.G.L., Bard, E., Bayliss, A., Beck, J.W., Bertrand, C., Blackwell, P.G., Buck, C.E., Burr, G., Cutler, K.B., Damon, P.E., Edwards, R.L., Fairbanks, R.G., Friedrich, M., Guilderson, T.P., Hughen, K.A., Kromer, B., McCormac, F.G., Manning, S., Ramsey, C.B., Reimer, R.W., Remmele, S., Southon, J.R., Stuiver, M., Talamo, S., Taylor, F.W., van der Plicht, J., Weyhenmeyer, C.E., 2004. INTCAL04 terrestrial radiocarbon age calibration, 0–26 cal kyr B.P. Radiocarbon 46, 1029–1058.

Reimer, P.J., Baillie, M.G.L., Bard, E., Bayliss, A., Beck, J.W., Blackwell, P.G., Bronk Ramsey, C., Buck, C.E., Burr, G.S., Edwards, R.L., Friedrich, M., Grootes, P.M., Guilderson, T.P., Hajdas, I., Heaton, T.J., Hogg, A.G., Hughen, K.A., Kaiser, K.F., Kromer, B., Mccormac, F.G., Manning, S.W., Reimer, R.W., Richards, D.A., Southon, J.R., Talamo, S., Turney, C.S.M., Van der Plicht, J., Weyhenmeyer, C.E., 2009. IntCal09 and Marine09 radiocarbon age calibration curves, 0–50,000 years cal BP. Radiocarbon 51, 1111–1150.

Rossetti, D.F., Goes, A.M., Valeriano, M.M., Miranda, M.C.C., 2007. Quaternary tectonics in a passive margin: Marajó Island, northern Brazil. Journal of Quaternary Science 22, 1–15.

Rossetti, D.F., Valeriano, M.M., Goes, A.M., Thales, M., 2008. Palaeodrainage on Marajó Island, northern Brasil, in relation to Holocene relative sea-level dynamics. The Holocene 18, 01–12.

Rossetti, D.F., Souza, L.S.B., Prado, R., Elis, V.R., 2012. Neotectonics in the northern equatorial Brazilian margin. Journal of South American Earth Sciences 37, 175–190.

Roubik, D.W., Moreno, J.E., 1991. Pollen and Spores of Barro Colorado Island, vol. 36. Missouri Botanical Garden, St. Louis.

Rull, V., Vegas-Vilarrùbia, T., Espinoza, N.P., 1999. Palynological record of an early-mid Holocene mangrove in eastern Venezuela: implications for sea-level rise and disturbance history. Journal of Coastal Research 15, 496–504.

Santos, M.L.S., Medeiros, C., Muniz, K., Feitosa, F.A.N., Schwamborn, R., Macedo, S.J., 2008. Influence of the Amazon and Pará Rivers on water composition and phytoplankton biomass on the adjacent shelf. Journal of Coastal Research 24, 585–593.

Sifeddine, A., Bertrand, P., Fournier, M., Martin, L., Servant, M., Soubiès, F., Suguio, K., Turcq, B., 1994. La sédimentation organique lacustre en milieu tropical humide (Carajás, Amazonie orientale, Brésil): relation avec les changements climatiques au cours des 60,000 dernières années. Bulletin de La Société Geologique de France 165, 613–621.

Sifeddine, A., Marint, L., Turcq, B., Volkmer-Ribeiro, C., Soubiès, F., Cordeiro, R.C., Suguio, K., 2001. Variations of the Amazonian rainforest environment: a sedimentological record covering 30,000 years. Palaeogeography, Palaeoclimatology, Palaeoecology 168, 221–235.

Smith, C.B., Cohen, M.C.L., Pessenda, L.C.R., França, M., Guimarães, J.T.F., Rossetti, D.F., 2011. Holocene coastal vegetation changes at the mouth of the Amazon River. Review of Palaeobotany and Palynology 168, 21–30.

Smith, C.B., Cohen, M.C.L., Pessenda, L.C.R., França, M.C., Guimarães, J.T.F., 2012. Holocenic proxies of sedimentary organic matter and the evolution of Lake Arari-Northern Brazil. Catena 90, 26–38.

Snedaker, S.C., 1978. Mangroves: their value and perpetuation. Natural Resources 16, 179–188.

Snedaker, S.C., 1982. Mangrove species zonation: why? In: Sen, D.N., Rajpurohit, K.S. (Eds.), Contributions to the Ecology of Halophytes, Tasks for Vegetation Science, Vol. 2. Junk, The Hague, pp. 111–125.

Solomon, A.M., Blasing, T.J., Solomon, J.A., 1982. Interpretation of floodplain pollen in alluvial sediments from an arid region. Quaternary Research 18, 52–71.

Spenceley, A.P., 1982. Sedimentation patterns in a mangal on Magnetic Island near Townsville, North Queensland, Australia. Singapore Journal of Tropical Geography 3, 100–107.

Stuiver, M., Reimer, P., Braziunas, T.F., 1998. High precision radiocarbon age calibration for terrestrial and marine samples. Radiocarbon 40, 1127–1151.

Sugita, S., 1994. Pollen representation of vegetation in quaternary sediments: theory and method in patchy vegetation. Journal of Ecology 82, 881–897.

Suguio, K., Martin, L., Bittencourt, A.C.S.P., Dominguez, J.M.L., Flexor, J.M., Azevedo, A.E.G., 1985. Flutuações do Nível do Mar durante o Quaternário Superior ao longo do Litoral Brasileiro e suas Implicações na Sedimentação Costeira. Revista Brasileira de Geociências 15, 273–286.

Sun, X., Li, X., 1999. A pollen record of the last 37 ka in deep sea core 17940 from the northern slope of the South China Sea. Marine Geology 156, 227–244.

Tomazelli, L.J., 1990. Contribuição ao Estudo dos Sistemas Deposicionais Holocênicos do Nordeste da Província Costeira do Rio Grande do Sul, com Ênfase no Sistema Eólico, Ph.D. Thesis, Universidade Federal do Rio Grande do Sul, Porto Alegre, Brasil.

Vedel, V., Behling, H., Cohen, M.C.L., Lara, R.J., 2006. Holocene mangrove dynamics and sea-level changes in Taperebal, northeastern Pará State, northern Brazil. Vegetation History and Archaeobotany 15, 115–123.

Versteegh, G.J.M., Schefuß, E., Dupont, L., Marret, F., Damsté, J.S.S., Jansen, J.H.F., 2004. Taraxerol and *Rhizophora* pollen as proxies for tracking past mangrove ecosystems. Geochimica et Cosmochimica Acta 68, 411–422.

Walker, R.G., 1992. Facies, facies models and modern stratigrahic concepts. In: Walker, R.G., James, N.P. (Eds.), Facies Models — Response to Sea Level Change. Geological Association of Canada, Ontario, Canada, pp. 1–14.

Walsh, G.E., 1974. Mangroves, a review. In: Reimold, R.J., Queens, W.H. (Eds.), Ecology of Halophytes. Academic Press, New York, NY, pp. 51–174.

Weng, C., Bush, M.B., Athens, J.S., 2002. Two histories of climate change and hydrarch succession in Ecuadorian Amazonia. Review of Paleobotany and Palynology 120, 73–90.

Wentworth, C.K., 1922. A scale of grade and class terms for clastic sediments. Journal of Geology 30, 377–392.

Woodroffe, C.D., Chappell, J., Thom, B.G., Wallensky, E., 1989. Depositional model of a macrotidal estuary and floodplains, South Alligator River, Northern Australia. Sedimentology 36, 737–756.

Xu, Q., Tian, F., Bunting, M.J., Li, Y., Ding, W., Cao, X., He, Z., 2012. Pollen source areas of lakes with inflowing rivers: modern pollen influx data from Lake Baiyangdian, China. Quaternary Science Reviews 37, 81–91.

Youssef, T., Saenger, P., 1999. Mangrove zonation in Mobbs Bay—Australia. Estuarine, Coastal and Shelf Science 49, 43–50.